Optics Communications 283 (2010) 1114–1123

Contents lists available at ScienceDirect

Optics Communications

journal homepage: www.elsevier.com/locate/optcom

Cascaded four-wave mixing in transparent bulk media

Jun Liu [a,b], Takayoshi Kobayashi [a,b,c,d,*]

[a] Department of Applied Physics and Chemistry and Institute for Laser Science, University of Electro-Communications, Chofugaoka 1-5-1, Chofu, Tokyo 182-8585, Japan
[b] JST, ICORP, Ultrashort Pulse Laser Project, 4-1-8 Honcho, Kawaguchi, Saitama, Japan
[c] Department of Electrophysics, National Chiao Tung University, 1001 Ta Hsueh Rd., Hsinchu 300, Taiwan
[d] Institute of Laser Engineering, Osaka University, Yamadakami 2-6, Suita 565-0871, Ibaraki 567-0047, Japan

ARTICLE INFO

Article history:
Received 7 July 2009
Received in revised form 28 October 2009
Accepted 28 October 2009

Keywords:
Cascaded four-wave mixing
Multicolor
Pulse self-compression

ABSTRACT

Cascaded four-wave mixing was theoretically and experimentally studied in transparent bulk media. The obtained sidebands show small angle dispersion, but have good beam quality with M^2 factor better than 1.1 in the measurement. The center wavelength of the generated multicolor sideband can be conveniently tuned by replacing the nonlinear medium with one of several different materials. Theoretical analysis and calculation based on the phase-matching condition with the consideration of broadband spectra of the two incident pulses clarified the mechanism of this process. Self-compressed multicolor 20-fs pulses, which were nearly transform-limited, were obtained when one of the two input beams was appropriately negatively chirped and the other was positively chirped.

1. Introduction

Wavelength-tunable laser pulses with ultrashort durations are needed to investigate the electronic and vibrational dynamics of atoms and molecules in a wide range of applications in the fields of photochemistry, physics, and biology [1,2]. There has been an ongoing effort to develop new and convenient methods for producing tunable ultrashort laser pulses. Four-wave mixing (FWM) has been studied in many various media and extensively used in a wide range of fields [3–5]. It has recently been studied in various optically transparent media as a new generation method of ultrabroadband and tunable ultrashort pulses [6–33]. Tunable visible ultrashort pulses were generated by FWM through filamentation in a gas cell [6]. Femtosecond pulses in deep UV and mid-IR have also been generated by FWM through filamentation or by using a hollow fiber in various gases [7–9].

It was recently discovered that ultrabroadband spectra and tunable ultrashort pulses can also be generated in various transparent bulk media [10–33]. In the case of solid-state bulk media, due to high material dispersion, phase-matching can be obtained only if the pump beams have a finite crossing angle in the media. By using picosecond pump pulses, highly efficient high-energy noncollinear four-wave optical parametric amplification was achieved in a transparent bulk Kerr medium [10,11]. Tunable mid-IR pulses were obtained in the range 2.4–7.7 μm using FWM in CaF_2 and BaF_2 plates [12]. Cascaded FWM sidebands were generated in BK7 glass [13], fused silica [14,15] and a sapphire plate [16,17] with two intersecting femtosecond laser beams. Sidebands extending from the UV to the near IR (a spectral range of more than 1.5 octaves) were obtained. Tunable multicolor femtosecond pulses with durations of about 45 fs were obtained in a fused silica plate when the two input beams were either positively chirped or not chirped [14,15]. Different-frequency resonant FWM, known as cascaded stimulated Raman scattering and coherent anti-Stokes Raman scattering, have been demonstrated, and sidebands with high-efficiency, broadband spectra have been generated in many nonlinear crystals including $PbWO_4$ [18], $LiNbO_3$ [19], $KNbO_3$ [20], TiO_2 [21], $KTaO_3$ [22,23], $YFeO_3$ [24], $SrTiO_3$ [25], diamond [26], and BBO [27]. As many as 20 anti-Stokes (AS) and two Stokes (S) coherent sidebands were generated by focusing dichromatic ultrashort pulses into a Raman-active crystal, lead tungstate ($PbWO_4$) [18,28]. A pair of isolated 25 fs and 13 fs pulses were obtained by combining these sidebands into a single beam in a $LiNbO_3$ crystal and $KTaO_3$ at room temperature, respectively [19,23].

In the present paper, the cascaded FWM was studied theoretically and experimentally in several transparent bulk media. We demonstrated that the center wavelength of the generated multicolor sidebands can be tuned by simply changing the nonlinear medium. Self-compressed multicolor femtosecond pulses with durations close to the transform-limited pulse width were obtained using cascaded FWM when one of the two input beams was negatively chirped and the other was positively chirped. A the-

* Corresponding author. Address: Department of Applied Physics and Chemistry and Institute for Laser Science, University of Electro-Communications, Chofugaoka 1-5-1, Chofu, Tokyo 182-8585, Japan. Tel.: +81 42 443 5845; fax: +81 42 443 5825.
E-mail address: kobayashi@ils.uec.ac.jp (T. Kobayashi).

0030-4018/$ - see front matter
doi:10.1016/j.optcom.2009.10.114

oretical analysis and calculation based on the phase-matching condition clarified the mechanism of this process. These calculation and analysis revealed why the frequency gap between two adjacent sidebands decreases as the order number increases.

2. Theoretical analysis

Cascaded FWM processes are schematically shown in Fig. 1a under the perfect phase-matching condition. The wave vectors of $\boldsymbol{k}_1$ and $\boldsymbol{k}_2$ are corresponding to the two input beams with respective frequencies of ω_1, ω_2 ($\omega_1 > \omega_2$). The cascaded FWM can be disassembled step by step as follows. In the first step, two $\boldsymbol{k}_1^{(1)}$ photons and one $\boldsymbol{k}_2^{(1)}$ photon generate a first-order anti-Stokes photon $\boldsymbol{k}_{AS1}$; the phase-matching condition of this FWM process can be described as $\boldsymbol{k}_{AS1} = 2\boldsymbol{k}_1^{(1)} - \boldsymbol{k}_2^{(1)}$ and $\omega_{AS1} = 2\omega_1^{(1)} - \omega_2^{(1)}$, as shown in Fig. 1b. Here, $\boldsymbol{k}_1^{(1)}$ and $\boldsymbol{k}_2^{(1)}$ are the wave vectors of the photons with the corresponding wavelength satisfying the phase-matching condition and frequency relation in the first FWM process. Then, succeeding FWM process among the generated $\boldsymbol{k}_{AS1}$ photon, one $\boldsymbol{k}_1^{(2)}$ photon and one $\boldsymbol{k}_2^{(2)}$ photon generate a second-order anti-Stokes photon $\boldsymbol{k}_{AS2}$. It is needed to note that the frequency and wave vector of $\boldsymbol{k}_1^{(2)}$ photon and $\boldsymbol{k}_2^{(2)}$ photon in this step are different from $\boldsymbol{k}_1^{(1)}$ photon and $\boldsymbol{k}_2^{(1)}$ photon that generated $\boldsymbol{k}_{AS1}$ photon. The phase-matching condition of this second step of cascaded FWM process is given by $\boldsymbol{k}_{AS2} = \boldsymbol{k}_{AS1} + \boldsymbol{k}_1^{(2)} - \boldsymbol{k}_2^{(2)} \approx 3\boldsymbol{k}_1^{(1)} - 2\boldsymbol{k}_2^{(1)}$, in which the directions of $\boldsymbol{k}_1^{(2)}$ and $\boldsymbol{k}_2^{(2)}$ are the same as those in $\boldsymbol{k}_1^{(1)}$ and $\boldsymbol{k}_2^{(1)}$ but their modulus are different. Because of the differences in wavelengths of $\boldsymbol{k}_1^{(2)}$ and $\boldsymbol{k}_2^{(2)}$ in the second process, the value of $\boldsymbol{k}_{AS2}$ is slightly different from $3\boldsymbol{k}_1^{(1)} - 2\boldsymbol{k}_2^{(1)}$. Therefore the value of $\boldsymbol{k}_{AS2}$ is given by $\boldsymbol{k}_{AS2} \approx 3\boldsymbol{k}_1^{(1)} - 2\boldsymbol{k}_2^{(1)}$ and the frequency is given by $\omega_{AS2} = \omega_{AS1} + \omega_1^{(2)} - \omega_2^{(2)} \approx 3\omega_1^{(1)} - 2\omega_2^{(1)}$, as shown in Fig. 1c. Subsequently, as shown in Fig. 1d, one $\boldsymbol{k}_{AS2}$ photon together with one $\boldsymbol{k}_1^{(3)}$ photon and one $\boldsymbol{k}_2^{(3)}$ photon generate a $\boldsymbol{k}_{AS3}$ photon; the phase-matching condition is $\boldsymbol{k}_{AS3} = \boldsymbol{k}_{AS2} + \boldsymbol{k}_1^{(3)} - \boldsymbol{k}_2^{(3)} \approx 4\boldsymbol{k}_1^{(1)} - 3\boldsymbol{k}_2^{(1)}$, $\omega_{AS3} = \omega_{AS2} + \omega_1^{(3)} - \omega_2^{(3)} \approx 4\omega_1^{(1)} - 3\omega_2^{(1)}$. To simplify the expression, the mth-order anti-Stokes sideband will have the following phase-matching condition: $\boldsymbol{k}_{ASm} = \boldsymbol{k}_{AS(m-1)} + \boldsymbol{k}_1^{(m)} - \boldsymbol{k}_2^{(m)} \approx (m+1)\boldsymbol{k}_1^{(1)} - m\boldsymbol{k}_2^{(1)}$, $\omega_{ASm} \approx (m+1)\omega_1^{(1)} - m\omega_2^{(1)}$. We need keep in mind that in every step, even the direction of $\boldsymbol{k}_1^{(m)}$ photon and $\boldsymbol{k}_2^{(m)}$ photon are the same, the frequency and wave vector value of $\omega_1^{(m)}$, $\omega_2^{(m)}$, $|\boldsymbol{k}_1^{(m)}|$, and $|\boldsymbol{k}_2^{(m)}|$ are different in every FWM step of m. On the Stokes side, two $\boldsymbol{k}_2^{(-1)}$ photons with one $\boldsymbol{k}_1^{(-1)}$ photon generate a first-order Stokes photon $\boldsymbol{k}_{S1}$, as shown in Fig. 1e. Then the generated $\boldsymbol{k}_{S1}$ photon together with a $\boldsymbol{k}_1^{(-2)}$ photon and a $\boldsymbol{k}_2^{(-2)}$ photon generate a second-order Stokes photon $\boldsymbol{k}_{S2}$. Therefore, the mth-order Stokes sideband will have the following phase-matching condition: $\boldsymbol{k}_{Sm} = \boldsymbol{k}_{S(m-1)} + \boldsymbol{k}_2^{(-m)} - \boldsymbol{k}_1^{(-m)} \approx (m+1)\boldsymbol{k}_2^{(-1)} - m\boldsymbol{k}_1^{(-1)}$, $\omega_{Sm} \approx (m+1)\omega_2^{(-1)} - m\omega_1^{(-1)}$. Thus, all the processes are FWM processes with third-order nonlinearity. Higher-order signals are obtained from the generated adjacent lower-order signals; hence the process is called *cascaded* FWM.

Fig. 1 shows that the required length of wave vector $|\boldsymbol{k}^{(m)}|$ for generating a FWM signal increases on both anti-Stokes and Stokes sides when the order number increases. For anti-Stokes beams, the wavelength is blue-shifted as the order number increases, which accords with the need of increasing length of $|\boldsymbol{k}^{(m)}|$. In this case, phase-matching can be achieved up to higher-order sidebands. However, the wavelengths of the Stokes beams increase with an increase of the order number. This red-shifted wavelength does not accord with the need of increasing length of $|\boldsymbol{k}^{(-m)}|$. As a result, the phase mismatch for the Stokes signal increases rapidly with the order number. Consequently, there are fewer Stokes sidebands than anti-Stokes sidebands generated in the output signal. The calculation described below gives the same result. We also can see that the maximum exit angle in the medium will be limited by the angle β (see Fig. 1b) on the anti-Stokes side due to the phase-matching condition. Based on the trigonometric formula, β can be expressed as: $\beta = \alpha + \sin^{-1}\left(|k_2|\sin\alpha / \sqrt{|k_1|^2 + |k_2|^2 - 2|k_1||k_2|\cos\alpha}\right)$, where α is the crossing angle between the two incident beams in the medium (see Fig. 1b).

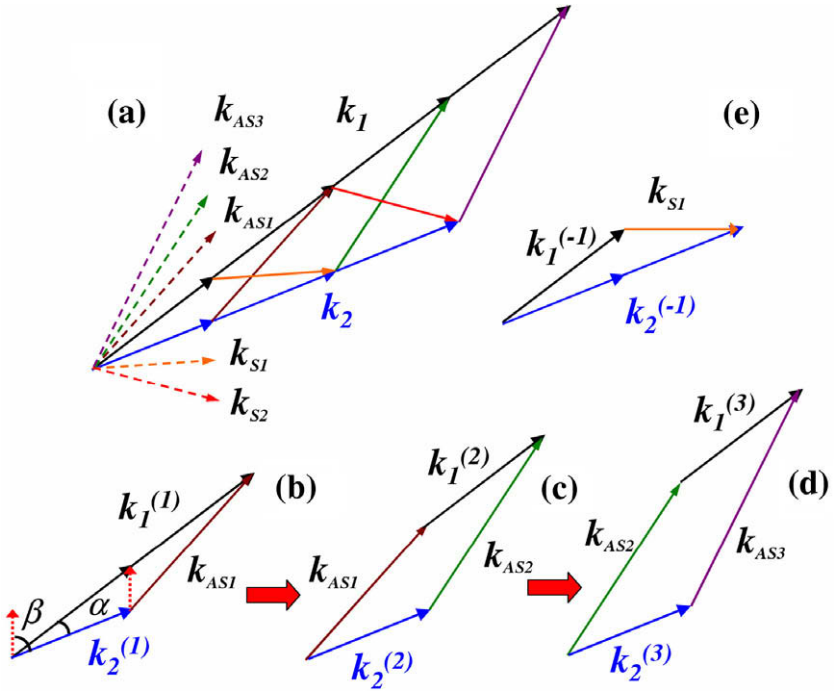

Fig. 1. (a) Phase-matching geometry for cascaded four-wave mixing process. Phase-matching geometries for generating (b) AS1, (c) AS2, (d) AS3, and (e) S1. $\boldsymbol{k}_1$ and $\boldsymbol{k}_2$ are the two input beams. The angle α is the crossing angle between the two input beams in the medium.

As for the generated signals, there are many routes for generating every sideband including the backward process as seen from Fig. 1a. In principle, every closed loop that includes the generated signal vector is a route. Take $\boldsymbol{k}_{AS2}$ as an example; there are many possible routes for generating $\boldsymbol{k}_{AS2}$: $\boldsymbol{k}_{AS2} = \boldsymbol{k}_{AS1} + \boldsymbol{k}_1^{(2)} - \boldsymbol{k}_2^{(2)}$, $\boldsymbol{k}_{AS2} = \boldsymbol{k}_1^{(1)} + \boldsymbol{k}_1^{(2)} - \boldsymbol{k}_{S1}$, $\boldsymbol{k}_{AS2} = \boldsymbol{k}_1^{(1)} + \boldsymbol{k}_1^{(1)} + \boldsymbol{k}_1^{(2)} - \boldsymbol{k}_2^{(1)} - \boldsymbol{k}_2^{(2)}$, $\boldsymbol{k}_{AS2} = \boldsymbol{k}_2^{(3)} + \boldsymbol{k}_{AS3} - \boldsymbol{k}_1^{(3)}$, and so on. In a medium, intrinsic fifth- and higher-order nonlinear processes are frequently ignored since the effects are much smaller than that third-order nonlinearity process. As described above, the higher-order Stokes signal is very weak due to the large phase mismatch and also because the crossing angle between the higher-order Stokes beam and the anti-Stokes beam is very large, making the interaction length short. Therefore, processes due to higher-order Stokes signals can also be ignored. Thus, the mth-order anti-Stokes signal is mainly generated by the cascading $\boldsymbol{k}_{ASm} = \boldsymbol{k}_{AS(m-1)} + \boldsymbol{k}_1^{(m)} - \boldsymbol{k}_2^{(m)}$ process. In the process, the contribution from the feedback process $\boldsymbol{k}_{ASm} = \boldsymbol{k}_{AS(m+1)} - \boldsymbol{k}_1^{(m)} + \boldsymbol{k}_2^{(m)}$ is small and can be neglected for higher-order signals. However, it is necessary to consider the contribution from the strong first-order Stokes or anti-Stokes signals for low-order anti-Stokes or Stokes signals. The small interference observable in the spectra of the low-order sidebands given in previous reports [16,27] demonstrates the importance of these two contributions.

3. Theoretical calculation

In previous experimental studies [13–18,26–29] and present work we found that the frequency difference between two adjacent sidebands decreased with increasing order number. Both input beams are femtosecond pulses and they thus have wide spectral bandwidths. As a result, different spectral band was selected from the broad input spectra, which induced this variable frequency gap between two adjacent sidebands with increasing order number. The following calculation explains this phenomenon semi-quantitatively. To simplify the calculation, we set the wavelength of one input beam to 800 nm (ω_2) (beam 2) and the wavelength of the other input beam to a wide bandwidth from 660 to 740 nm with a center wavelength at 700 nm (ω_1) (beam 1); this accords with the frequency parameters for the two input beams in our experiment [14]. For a given external crossing angle in the same material, the frequencies and wave vectors of cascaded FWM sidebands are determined by the phase-matching conditions: $\boldsymbol{k}_{ASm} = \boldsymbol{k}_{AS(m-1)} + \boldsymbol{k}_1^{(m)} - \boldsymbol{k}_2^{(m)}$, $\omega_{ASm} = \omega_{AS(m-1)} + \omega_1^{(m)} - \omega_2^{(m)}$ and $\boldsymbol{k}_{Sm} = \boldsymbol{k}_{S(m-1)} + \boldsymbol{k}_2^{(-m)} - \boldsymbol{k}_1^{(-m)}$, $\omega_{Sm} = \omega_{S(m-1)} + \omega_2^{(-m)} - \omega_1^{(-m)}$. We calculated this process step by step. In every step of cascaded FWM process, we scan the wavelength of ω_1 from 660 to 740 nm to find the minimum phase mismatching $\Delta\boldsymbol{k}_{ASm} = \boldsymbol{k}_{AS(m-1)} + \boldsymbol{k}_1^{(m)} - \boldsymbol{k}_2^{(m)} - \boldsymbol{k}_{ASm}$ or $\Delta\boldsymbol{k}_{Sm} = \boldsymbol{k}_{S(m-1)} + \boldsymbol{k}_2^{(-m)} - \boldsymbol{k}_1^{(-m)} - \boldsymbol{k}_{Sm}$. For example, from Fig. 1b, the phase mismatch $\Delta\boldsymbol{k}_{AS1}$ depends only on the wavelength of ω_1 from 660 to 740 nm when all the other input parameters are fixed. Then, the output parameters, including direction and wavelength, of the first-order sideband (AS1) can be determined by finding the minimum phase mismatch $\Delta\boldsymbol{k}_{AS1}$ when scanning the wavelength of ω_1 from 660 to 740 nm. After the parameters of AS1 have been determined, the output parameters of AS2 can be determined in the same way of finding the minimum phase mismatch $\Delta\boldsymbol{k}_{AS2}$ through scanning the wavelength of ω_1 from 660 to 740 nm, as shown in Fig. 1c. It can be concluded that all the output parameters of the sidebands can be determined by finding the minimum phase mismatch $\Delta\boldsymbol{k}_{ASm}$ or $\Delta\boldsymbol{k}_{Sm}$. In this way, we can calculate the exit angle and wavelength of the generated cascaded FWM sidebands, the wavelength of ω_1 at the minimum phase mismatch, and the minimum phase mismatching for every step of cascaded FWM.

Here, we calculated the output parameters of the generated sidebands when the material is a 1-mm fused silica plate for several external crossing angles (1.40°, 1.64°, 1.87°, 2.10°, 2.34°, and 2.57°) which are the same conditions as those in Ref. [14]. Fig. 2 shows the calculation results, where an order number of 0 refers to beam 2 with 800 nm (ω_2), an order number of 1 refers to the wavelength of beam 1 between 660 and 740 nm (ω_1) when the minimum phase mismatching $\Delta\boldsymbol{k}_{AS1}$ are obtained, and an order number of 2 refers to the first-order anti-Stokes sideband (AS1), etc. Fig. 2a shows the wavelength of beam 1 for generating different order sidebands in the case of the phase mismatching is the minimum. In Fig. 2a, the order numbers 0 and 1 refer to beam 2 and beam 1, respectively. The wavelength related to order number 2 refers to the wavelength of ω_1 for generating AS1 in the case of the phase mismatching is the minimum, and so on. We can see that the optimal external crossing angle that the minimum phase mismatching for AS1 was obtained at the center wavelength of ω_1 700 nm in this case is about 1.87° which is accord with the experiment data. The wavelength of beam 1 increases with the order number of the anti-Stokes sideband. This explains why the wavelength gap between two adjacent sidebands decreases with increasing order number. For the higher-order numbers, the frequency difference between two adjacent sidebands becomes equal. This is because the two input pulses have limited spectral bands. The wavelength of beam 1 increases and fixed at the maximum wavelength of 740 nm in this calculation at higher-order numbers (see Fig. 2a). For the same order number, the wavelength difference of ω_1 induces also a different wavelength gap between two adjacent sidebands for different external crossing angles. We also can see that the wavelength of beam 1 decreases for the same-order sideband with the increase of the external crossing angles. This is the reason that the spectra of the generated sidebands are tunable by changing the external crossing angles. It also can explain the evolution of output power of sidebands at different external crossing angle in Fig. 4a in Ref. [14]. It is because both input pulses have Gaussian spectral profile that the highest intensity of ω_1 locate at center wavelength 700 nm and decreasing on both sides. Then, the output power of the sideband will be higher when the wavelength of ω_1 close to 700 nm and lower when it far from 700 nm. When the external crossing angle is 1.4°, the S1 and AS1 have high output power and decreasing quickly with the order number increasing. When the external crossing angle is 1.87°, the S1 and AS1 also have high output power. However, the output powers from AS2 to AS5 are higher and decreasing more slowly with the order number increasing compare with that at 1.4° crossing angle. These results in accords with wavelength of ω_1 in Fig. 2a. We can see that it can be explained in the same way when the external crossing angles are 2.10° and 2.57°. It explains that it is difficult to obtain higher-order Stokes sideband. Fig. 2b shows the evolution of the wavelength of the generated sidebands with the order number at several different external crossing angles (1.40°, 1.64°, 1.87°, 2.10°, 2.34°, and 2.57°). It clearly shows that the wavelength of the same order sideband can be tuned by changing the external crossing angle. Fig. 2c shows the exit angles of different sidebands at several different external crossing angles, the evolution agrees well with the experiment data given in Ref. [14]. Fig. 2d shows the curve of the dependence of the exit angle of the generated sidebands on the center wavelength of generated sidebands for several different media. It is interesting to see that the curves are almost overlapped for different external crossing angles for the same medium. Here, in Fig. 2d, we only display the curves at 1.40°, 1.87°, and 2.57° three different angles. This result is in accordance with Fig. 4 in Ref. [27]. Fig. 2e shows the phase mismatching in 1 mm thick fused silica from AS1 to AS4 at 1.87° and 2.34°. The slope of the curves increased with the order number increasing. It means that the gain bandwidth of the sideband will decrease with the order

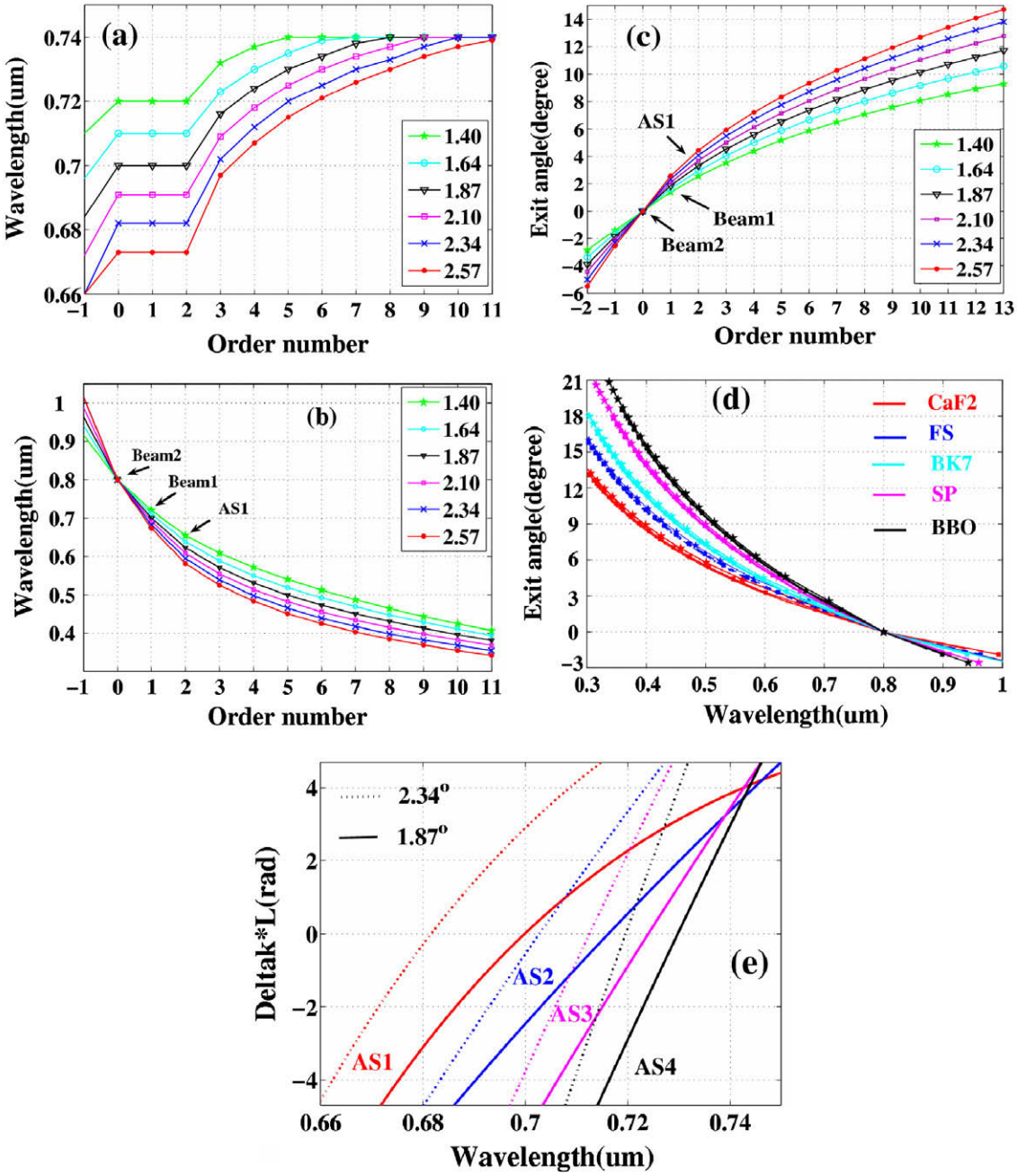

Fig. 2. Dependence of (a) the wavelength of generated sidebands, (b) the wavelength of beam 1 for optimal phase-matching, and (c) the exit angles of the generated sidebands on the order number at six different crossing angles (1.40°, 1.64°, 1.87°, 2.10°, 2.34°, and 2.57°) in a 1-mm thick fused silica plate. (d) The dependence of the exit angle of the generated sidebands on the center wavelength of generated sidebands at 1.40°, 1.87°, and 2.57° three different crossing angles in five different media (CaF_2, fused silica, BK7, sapphire plate, and BBO crystal). (e) The phase mismatching in 1 mm thick fused silica from AS1 to AS4 at 1.87° and 2.34°.

number increasing for the same crossing angle. The slope increases also with the input crossing angle for the same sideband.

Fig. 3a shows the dependence of the wavelength of every sideband on the order number at several different transparent bulk media (CaF_2, fused silica, BK7, sapphire plate, and BBO crystal) when the crossing angle fixed at 1.8°. It is obvious that the wavelength of every sideband is tunable at a fixed external crossing angle in various transparent bulk media. This means that the center wavelength of the generated multicolor sideband can be conveniently tuned by simply replacing the nonlinear medium. We also calculated the group delay between beam 2 (800 nm) and other wavelength in CaF_2, fused silica, BK7, and sapphire plate, as shown in Fig. 3b. If we want to obtain broadband sidebands [32,33], it can be concluded that it is more advantageous to use a bulk medium with low dispersion, for example CaF_2 and fused silica, and use a thin (~150 μm) glass as the nonlinear medium in the process to reduce time delay.

The above calculations are all based on the phase-matching condition which only indicates the important role of the phase-matching in this process. Although it can qualitatively explain the process, this is inadequate when the two input pulses are femtosecond pulses with broadband spectrum. For a much more precise description and to understand the process fully, the analysis should begin with an integral description of the FWM nonlinear polarization density just the same as Refs. [34,35]. The third-order dielectric polarization induced at frequency Ω by the input beams can be ex-

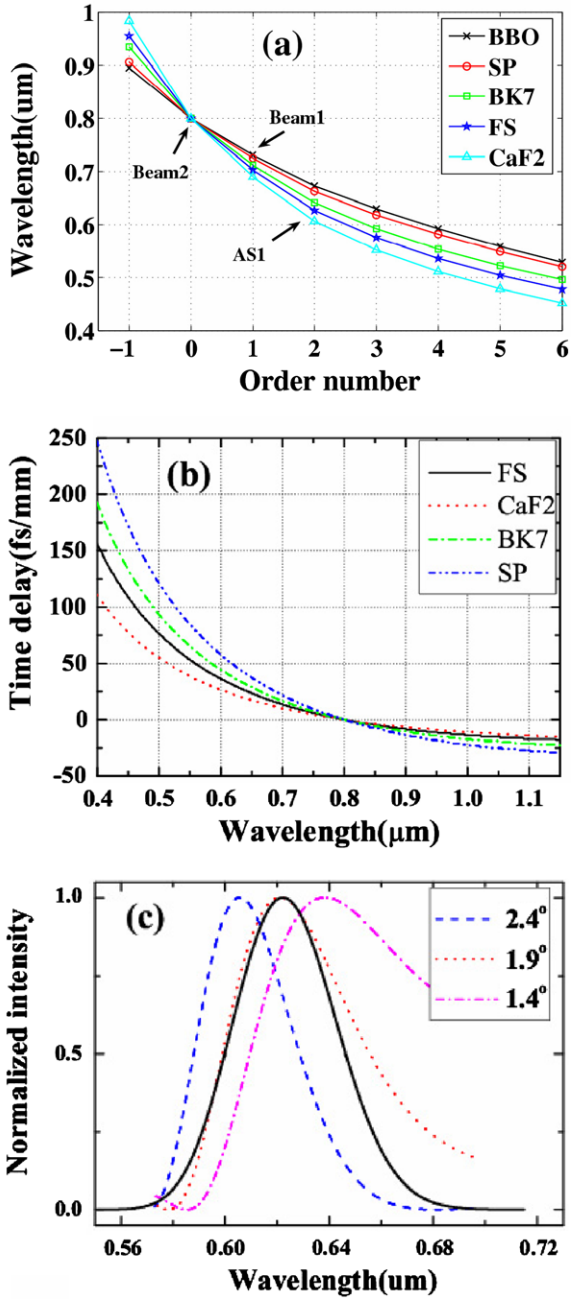

Fig. 3. (a) Dependence of the wavelength of generated sidebands on the order number in five different media (CaF_2, fused silica, BK7, sapphire plate, and BBO crystal) when the crossing angle is 1.8°. (b) The group delay between beam 2 (800 nm) and other wavelength in CaF_2, fused silica, BK7, and sapphire plate with 1 mm thickness. (c) The black solid line is the ideal AS1 signal intensity. The dash-dot line, dotted line, and short-dashed line refer to curves related to phase mismatching $\mathrm{sinc}^2(\Delta k_z(\Omega,\omega_1,\omega_2)L/2)$ at 1.4°, 1.9°, and 2.4°, respectively.

pressed by summing over all possible permutations of the input frequencies according to the third-order susceptibility [35]:

$$\tilde{P}^{(3)}(z,\Omega) = \iint d\omega_1 d\omega_2 \tilde{\chi}^{(3)}(\omega_{eg}-\omega_1,\omega_1-\omega_2, -\omega_{eg}+\Omega)\tilde{E}_1^*(z,\omega_1)\tilde{E}_2(z,\omega_2)\tilde{E}_3(z,\Omega-\omega_2+\omega_1) \times \exp[i(-k_{1z}(\omega_1)+k_{2z}(\omega_2)+k_{3z}(\Omega-\omega_2+\omega_1))z]. \quad (3.1)$$

In the expression, we assume the pulses are overlapped very well in time. Representation of the frequency-dependent third-order non-

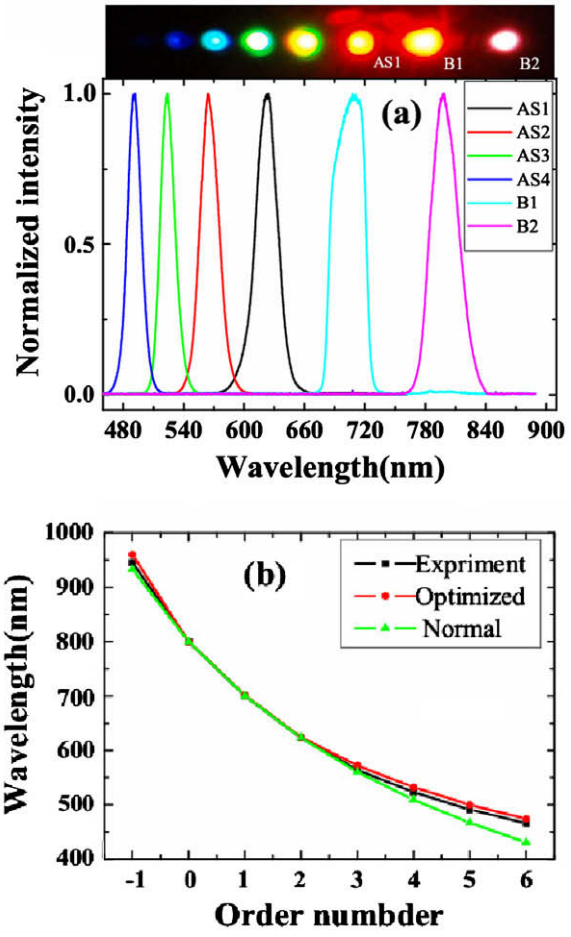

Fig. 4. (a) The curves are spectra of the sidebands from AS1 through AS4 and two input beams when the crossing angle between the two input beams is 1.8°. B1 and B2 refer to beam 1 and beam 2, respectively. The top picture of Fig. 4a is a photograph of the sidebands on a sheet of white paper behind a 1-mm thick fused silica plate. (b) Dependence of sideband wavelength on the order number: experimental result (black square line), optimized theoretical result considering the spectral bandwidth of input pulses (red circle line), and theoretical result without considering the spectral bandwidth (green triangle line), where an order number of 0 refers to beam 2, an order number of 1 refers to beam 1, and an order number of 2 refers to AS1, etc.

linear susceptibility, $\tilde{\chi}^{(3)}(\omega_{eg}-\omega_1,\omega_1-\omega_2,-\omega_{eg}+\Omega)$, is based on the interaction of the input fields with an electronic transition with the frequency ω_{eg}. In the case of a nonlinear process with a low efficiency ($E_{1,2,3} = const$), the four-wave mixing signal field can be obtained through integrate the signal intensity over the longitudinal coordinate z, as follows:

$$\begin{aligned}\tilde{E}_4(L,\Omega) &= i\frac{c\mu_0\Omega}{2n_4(\Omega)}\int_0^L \tilde{P}^{(3)}(z,\Omega)\exp(-ik_{4z}(\Omega)z)dz \\ &= i\frac{c\mu_0\Omega L}{2n_4(\Omega)}\iint d\omega_1 d\omega_2 \tilde{\chi}^{(3)}(\omega_{eg}-\omega_1,\omega_1-\omega_2, \\ &\quad -\omega_{eg}+\Omega)\tilde{E}_1^*(z,\omega_1)\tilde{E}_2(z,\omega_2)\tilde{E}_3(z,\Omega-\omega_2+\omega_1) \\ &\quad \times \sin c(\Delta k_z(\Omega,\omega_1,\omega_2)L/2)\exp(i\Delta k_z(\Omega,\omega_1,\omega_2)L/2).\end{aligned} \quad (3.2)$$

Here, $\Delta k_z(\Omega,\omega_1,\omega_2) = -k_{1z}(\omega_1)+k_{2z}(\omega_2)+k_{3z}(\Omega-\omega_2+\omega_1)-k_{4z}(\Omega)$ is the phase mismatch, L is length of medium. As a result, the obtained four-wave mixing signal intensity can be expressed:

$$I_4^{(3)}(\Omega) = \frac{\varepsilon_0 n_4(\Omega)Q(\Omega)}{c}|\tilde{E}_4(L,\Omega)|^2 \propto R(\Omega)I_4^{ideal}(\Omega), \quad (3.3)$$

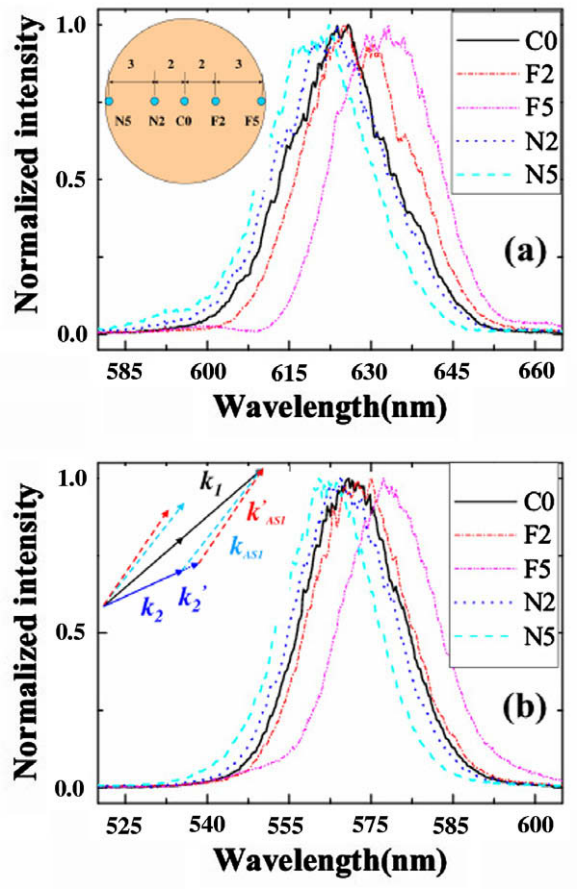

Fig. 5. The inset pattern in figure (a) shows the five different positions on the beam we measured. C0 is the center of the beam. N5 and N2 refer to the side close to the two input beams. F2 and F5 refer to the side far from the two input beams. (a) and (b) show the spectra at the five different positions on the AS1 and AS2 sidebands, respectively. The inset of (b) shows the phase-matching geometry which indicates longer wavelength on the side far from the two input beams.

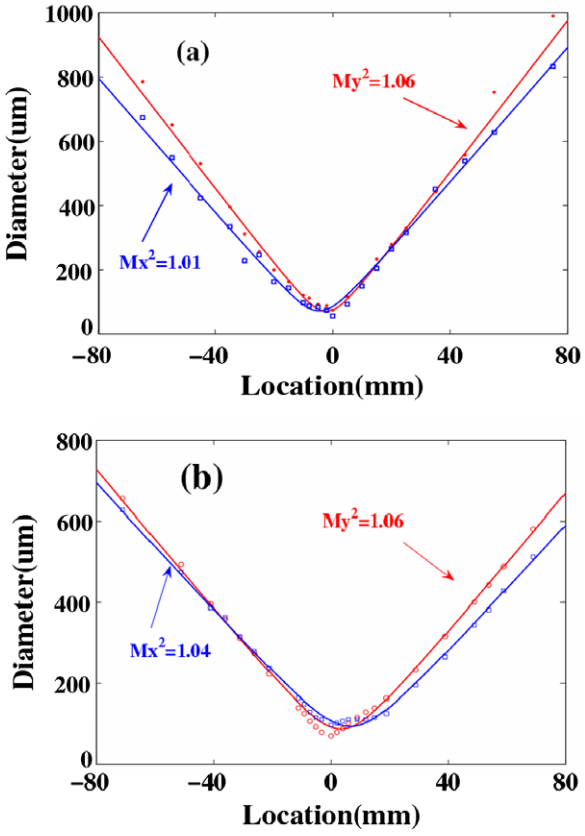

Fig. 6. Measured beam diameters and M^2 in both *X* and *Y* directions for (a) AS1 and (b) AS2 sideband, respectively.

where c is the vacuum light speed. $n_4(\Omega)$ is the index of generated signal at frequency Ω. $Q(\Omega)$ is the response function of the detector. $I_4^{ideal}(\Omega)$ is an ideal four-wave mixing signal intensity and can be expressed:

$$I_4^{ideal}(\Omega) = \left| \iint d\omega_1 d\omega_2 \tilde{E}_1^*(z,\omega_1)\tilde{E}_2(z,\omega_2)\tilde{E}_3(z,\Omega-\omega_2+\omega_1) \right|^2 \tag{3.4}$$

and

$$R(\Omega) = \frac{Q(\Omega)\Omega^2}{n_4(\Omega)} \sin c^2(\Delta k_z(\Omega,\omega_1,\omega_2)L/2). \tag{3.5}$$

In the calculation, the input parameters are the same as above calculation. The ideal AS1 signal intensity was shown in Fig. 3c with black solid line. The curves related to phase mismatching $\sin c^2(\Delta k_z(\Omega,\omega_1,\omega_2)L/2)$ at 1.4°, 1.9°, and 2.4° were shown in Fig. 3c with dash-dot line, dotted line, and short dash line, respectively. The same as above calculation, the phase mismatching was calculated through fixed one wavelength of beam 1 and scan the wavelength of beam 2 in several spectral bandwidth region in a 0.2 mm fused silica glass. It shows obviously the dependence of the spectrum of AS1 on the crossing angle of the two input beams. We can see that the output wavelength not only dependent on the phase mismatching but also the ideal curve (or the spectra of input pulses). The same as description in Refs. [34,35], $\frac{Q(\Omega)\Omega^2}{n_4(\Omega)}$ will also introduce blue-shift of the signal wavelength. As a result, the center wavelength of the generated sideband was not exact the wavelength that the phase mismatching was zero but a little shift to the center wavelength of the ideal spectrum.

4. Experiment

The experimental setup is the same as that in used in previous studies [14,15]. The source was a Ti:sapphire regenerative amplifier laser system (Legend-USP, Coherent) with a pulse duration of 40 fs, 1-kHz repetition rate, and an average power of 2.5-W. The laser pulse was split into several beams. One of the beams (beam 1) was spectrally broadened in a 60-cm hollow fiber with an inner diameter of 250 μm that was filled with krypton gas. The broadband spectrum after the hollow fiber was dispersion compensated using a pair of chirped mirrors and a pair of glass wedges. The pulse was negatively chirped by the chirped mirror pairs. After passing through a 40-nm-bandpass filter centered at 700 nm, beam 1 was focused into a transparent bulk medium by a 60-cm-focal-length concave mirror. Another beam (beam 2) passed through a delay stage having a resolution of less than 3 fs. Beam 2 was first attenuated by a variable neutral density (VND) filter and it was then focused into the transparent bulk medium by a 1-m focal-length lens. Positive chirp was induced due to the dispersions in lenses, beam splitters, and a VND filter. A third beam (beam 3) was used to measure the pulse duration using the cross-correlation frequency resolved optical gating technique by mixing it with the two input beams or the generated sidebands in a 10-μm thick BBO crystal.

The pulse duration of beam 2 was 75 fs with positive chirp, while that of beam 1 was 50 fs with negative chirp. The input power of beam 1 (beam 2) was 8 (24) mW and its diameter on

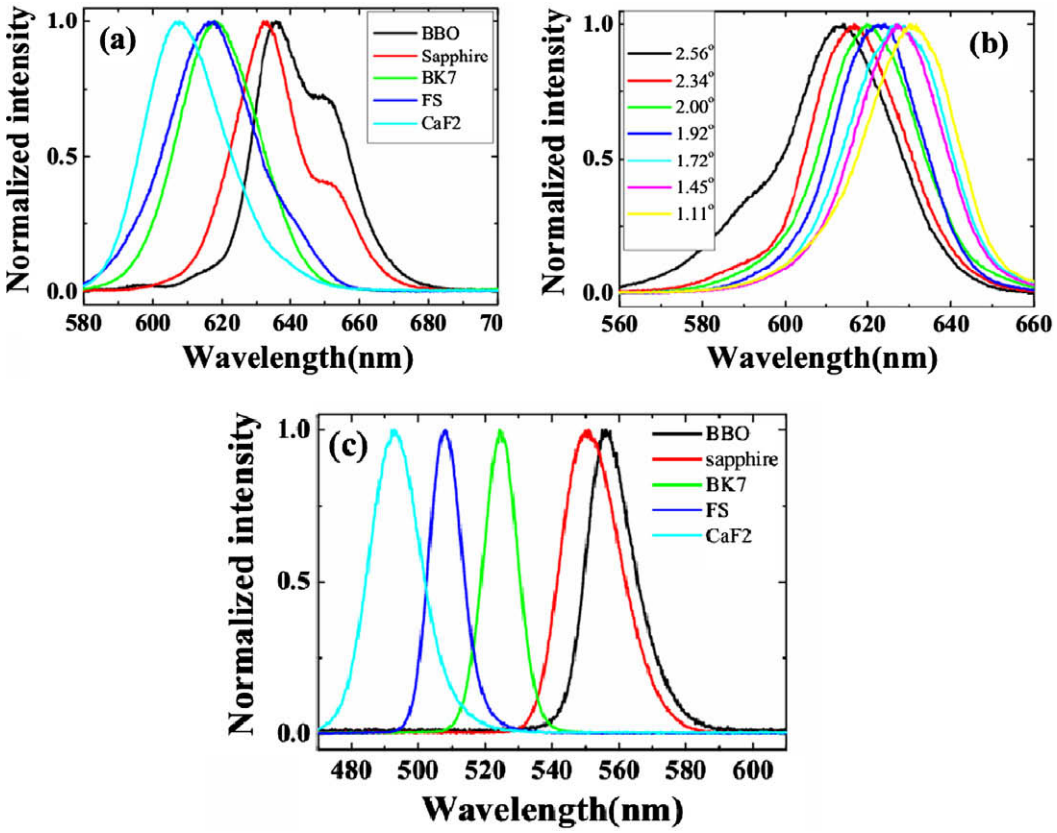

Fig. 7. Spectra of (a) the first-order anti-Stokes sideband (c) the third-order anti-Stokes sideband of CaF_2, fused silica, BK7, sapphire plate, and BBO crystal at 1.8° crossing angle. (b) Spectra of the first-order anti-Stokes sideband of fused silica at different crossing angles in the range 1.11°–2.56°.

the surface of the transparent bulk medium was 250 μm (300 μm) in the vertical direction and 300 μm (550 μm) in the horizontal direction, as measured using a CCD camera (BeamStar FX33, Ophir Optronics). The beam intensities on the glass surface were more than one order of magnitude lower than the optical breakdown threshold for all of the transparent bulk media used and no damage was found during or after irradiation by the beams. Both input beams were horizontally polarized. The position of beam 2 was fixed and the crossing angle between beams 1 and 2 was varied with a precision of ±0.02° by adjusting the position of beam 1 on the surface of a concave mirror in front of the transparent bulk medium.

5. Results and discussion

As beams 1 and 2 were synchronously focused on the transparent bulk medium in time and overlapped in space, separate cascaded FWM signals at different wavelengths were generated and they were well separated in a line next to the input beams. The top of Fig. 4a shows a photograph of the FWM sideband spots on a white sheet of paper behind a 1-mm thick fused silica plate. Cascaded signals could be obtained from plates as thin as 150 μm if the peak intensity on the glass surface exceeded 2 TW cm^{-2} [13]. The first, second, and third spots in the figure from the right-hand edge are beam 2, beam 1, and AS1, respectively. The signal beam profiles of the sidebands have good Gaussian mode patterns. Fig. 4a shows the spectra of the sidebands and the two input beams. B1 and B2 refer to beams 1 and 2, respectively. All the spectra of the sidebands have smooth profiles. The dependence of the wavelengths of different sidebands on the order number is shown in Fig. 4b. The experiment data accords with the optimized calculation that the broad spectra of the input pulses are considered. The slightly shift between the experimental and optimized calculation data due to the Gaussian profile of the spectra of the two input pulses. If the spectral bandwidth of the input pulses were not considered $\omega_{ASm} = (m+1)\omega_1^{(1)} - m\omega_2^{(1)}$, the wavelength error of the same order sideband between the normal calculation and experimental results increased with increasing order number, as shown in Fig. 4b (green[1] triangle line).

In the experiment, we measured the spectra of AS1 and AS2 at five different positions on the sideband, as shown in the inset of Fig. 5a. The beam diameter was expanded to about 11 mm after propagating about 1.5 m in the air. C0 was the center measurement position. N2 and N5 were the two positions 2 mm and 5 mm, respectively, away from C0 on the side close to the input beams. F2 and F5 were the two positions on the side far from the input beams. Fig. 5a and b demonstrated the normalized spectra profile at N5, N2, C0, F2, and F5 five different positions on the AS1 and AS2 sideband, respectively. All the spectra owed nice Gaussian profile for different positions. Longer wavelength located on the position far away from the two input beams and the shorter wavelength generated on the position close to the two input beams. The center wavelength was shifted for about 15 nm between the two edge points F5 and N5. It indicated that there was small angle dispersion in the sidebands. The angle dispersion can be explained by the different angles for phase-matching condition to be deflected upon transmission from the crystal to air, as shown in inset of Fig. 5b.

The M^2 factors of AS1 and AS2 were measured using a CCD camera (BeamStar FX33, Ophir Optronics) to measure the beam diameters at more than 10 different positions on both sides of the focal

[1] For interpretation of color in Figs. 1-8, the reader is referred to the web version of this article.

Table 1
The output power of different sidebands for several different bulk media when the external crossing angle is about 1.8°. In the case, the input power of beam 1 and beam 2 are 7 mW and 25 mW, respectively.

	CaF_2 (μW)	Fused silica (μW)	BK7 (μW)	Sapphire plate (μW)	BBO (μW)
AS1	480	700	715	750	780
AS2	210	315	295	210	135
AS3	125	90	60	40	10

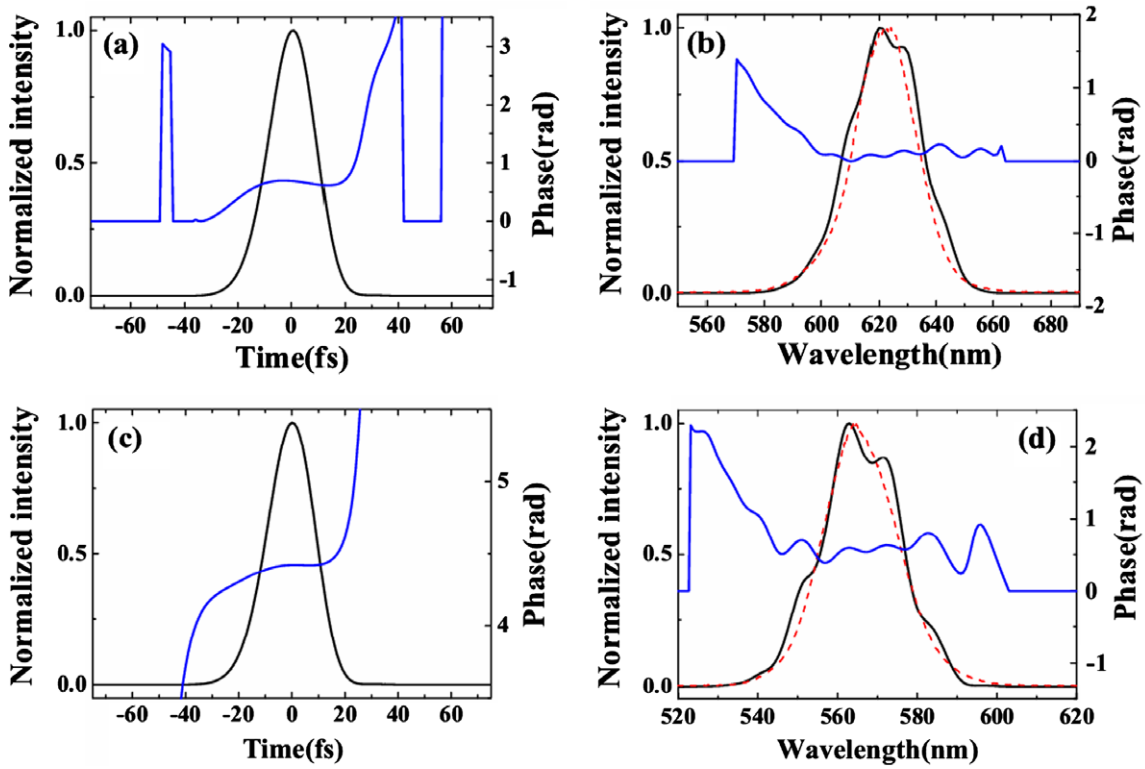

Fig. 8. Recovered intensity profile and phase of (a) AS1 and (c) AS2. Recovered spectrum (black solid curve), spectral phase (blue solid curve), and measured spectrum (red dotted curve) of (b) AS1 and (d) AS2.

point. The measured beam diameter data were curve fitting into hyperbola and obtained the value of M^2 factor [36,37]. Fig. 6a shows the obtained M^2 factor value of AS1 at X and Y directions were about 1.01 and 1.06, respectively. Fig. 6b shows that the M^2 factor value of AS2 at X and Y directions were about 1.04 and 1.06, respectively. Both AS1 and AS2 owed perfect beam quality. These good beam qualities owe to the soliton effect in the mixing process [38,39].

In the experiment, we replaced the fused silica plate with other transparent bulk media: a CaF_2 plate, a BK7 glass plate, a sapphire plate, and a BBO crystal cut at $\theta = 20.4°$, $\phi = 0°$ (o light) all with a thickness of 1 mm. When the two input beams were the same and the crossing angle was fixed at 1.8°, the spectra for the same order sideband differed greatly for the different transparent bulk media. Fig. 7a shows the spectra of the first-order anti-Stokes signals for transparent bulk medium of CaF_2, fused silica, BK7, sapphire plate, and BBO crystal. The signal generated by CaF_2 has the shortest wavelength among them, while the BBO crystal induces the longest wavelength signal. Fig. 7b shows the spectra of the first-order anti-Stokes sideband for fused silica by varying the crossing angle between 1.11 and 2.56°. As mentioned above, the difference in the center wavelength increases as the order number increases. Fig. 7c shows the spectra of the third-order anti-Stokes signals of CaF_2, fused silica, BK7, sapphire plate, and BBO crystal. The difference in the center wavelengths of CaF_2 and BBO crystal increased from 40 nm to about 65 nm. The wavelength ranges of different order signals from different bulk media overlap with each other. This means it is possible to continuously tune the spectrum both by simply replacing the medium and by varying the crossing angle. Table 1 showed the output power of different sidebands for several different bulk media when the external crossing angle is about 1.8°. In the case, the input powers of beam 1 and beam 2 were 6.5 mW and 25 mW, respectively. Even the output power of AS1 was the lowest for CaF_2, the powers of AS2 and AS3 were still very high. For BBO, the power of the sideband decreased quickly as the order number increase. This output power dependent phenomenon was almost the same as that of by changing the external crossing angle in Fig. 4a in Ref. [14]. In the case, 1.8° is a large crossing angle for CaF_2 and a small angle for BBO.

Self-compressed multicolor femtosecond pulses that were nearly transform-limited were obtained when beam 1 was negatively chirped ($\partial^2\phi_1(t)/\partial t^2 < 0$) and beam 2 ($\partial^2\phi_2(t)/\partial t^2 > 0$) was positively chirped. By using the phase-matching condition: $\boldsymbol{k}_{AS1} = 2\boldsymbol{k}_1 - \boldsymbol{k}_2$ and $\omega_{AS1} = 2\omega_1 - \omega_2$, the leading edges of the up-shifted anti-Stokes sidebands (AS1) will have shorter wavelengths when the two chirped input beams are focused into a medium to generate cascaded FWM sidebands. As a result, the anti-Stokes sidebands will be negatively chirped. This can be described using

following expressions [29]. Both chirped input pulses can be written as:

$$E_1(t) \propto \exp\{i[\omega_{10}t + \phi_1(t)]\}, \quad E_2(t) \propto \exp\{i[\omega_{20}t + \phi_2(t)]\}.$$

The mth ($m > 0$) order anti-Stokes signal can be expressed as:

$$E_{ASm}(t) \propto \exp\{i[((m+1)\omega_{10} - m\omega_{20})t + ((m+1)\phi_1(t) - m\phi_2(t))]\}$$

and

$$\partial^2\phi_{ASm}(t)/\partial t^2 = (m+1)\partial^2\phi_1(t)/\partial t^2 - m\partial^2\phi_2(t)/\partial t^2 < 0.$$

Given $\partial^2\phi_1(t)/\partial t^2 < 0$ and $\partial^2\phi_2(t)/\partial t^2 > 0$, the mth-order anti-Stokes signal is also negatively chirped. Nearly transform-limited pulses could be achieved when the negative chirp of the anti-Stokes sidebands just compensates the dispersion of the transparent bulk media, group velocity delay of two pump pulses induced phase change, and the nonlinear phase change in the medium. This method can be used in all FWM process.

The pulse durations of AS1 and AS2 were measured by XFROG. The spectral and temporal profile and the phase were retrieved using a commercial software (FROG 3.0, Femtosoft Technologies) with a 256 × 256 grid. The retrieval error was smaller than 0.010. Fig. 8a and c shows the temporal profiles and phases of AS1 and AS2. The pulse durations of AS1 and AS2 are 20 fs and 22 fs respectively, which are very close to the transform-limited pulse durations of AS1 and AS2 (18 fs and 19 fs, respectively). It is obvious that the spectrum of the sideband can also a little be broadened due to the chirp of the input pulses. The nonlinear phase changes in the medium combine with 1-mm thick compensate the chirps of the generated sidebands. The obtained pulse duration is a factor of two shorter than that obtained in a previous report for about 45 pulses with nearly no chirped pulse input [14]. The obtained pulse durations are even shorter than the transform-limited pulse durations of the two input beams, which are 32 fs and 33 fs for beams 1 and 2, respectively. Fig. 8b and d shows the retrieved spectra and the spectral phases of AS1 and AS2, respectively. The retrieved spectra reproduced the measured spectra very well. The retrieved phase shows a small positive chirp and some high-order dispersion. No dispersive compensation in the optical component for the output sideband was used in this process. In the process, the 1-mm glass can only induce limited dispersion that can compress the pulse for about 1 fs in this case. Then, the group velocity delay between two input pulse and the nonlinear phase in the process maybe contribute the compression a lot. More detail analysis will be done through numerical simulation in the future.

6. Conclusion and future prospect

In conclusion, the cascaded FWM process was theoretically analyzed and an experiment was performed using several different bulk transparent media. Theoretical analysis and calculation based on the phase-matching condition taking into account of the broadband spectra of the two incident pulses explained puzzling phenomena at first glance taking place in this process. The obtained sidebands show small angle dispersion and perfect beam quality with M^2 factor better than 1.1. The wavelength of the generated multicolor sidebands can be conveniently tuned by simply replacing the medium. Self-compressed multicolor femtosecond pulses that were nearly transform-limited were obtained when one of the two input beams was negatively chirped and the other was positively chirped. Dispersive compensation is not needed to obtain compressed pulses in this process. In addition, there are several other features of using cascaded FWM to generate tunable femtosecond pulses:

First, several up- and down-shifted multicolor femtosecond pulses can be simultaneously obtained and spatially separated from the input beams. They are thus self-synchronized and convenient for multicolor pump–probe experiments [40], femtosecond CARS spectroscopy [41] and two-dimensional spectroscopy [42].

Second, FWM can be applied more universally to nearly all transparent media over a broad wavelength range from UV to MIR.

Third, cascaded FWM can in principle be scaled up to much higher energies if the energies of the two input beams are high enough because there is no theoretical limit to the size of the glass materials used.

Fourth, the M^2 factor of the generated sideband using cascaded FWM can be less than 1.1 in our measurement, which indicates a perfect beam quality.

Furthermore, these broadband sidebands can be used to obtain near single cycle pulse chain through Fourier synthesis of the sidebands [19,23,32,33]. If the input beams are carrier-envelope phase (CEP) stabilized, all the generated sidebands would be CEP stabilized. As a result, CEP stabilized near single cycle pulse chain can be obtained in this way [32].

Acknowledgements

This work was partly supported by the 21st Century COE program on "Coherent Optical Science" and partly supported by the grant from the Ministry of Education (MOE) in Taiwan under the ATU Program at National Chiao Tung University. A part of this work was performed under the joint research project of the Laser Engineering, Osaka University, under contract subject B1-27.

References

[1] A.H. Zewail, J. Phys. Chem. A 104 (2000) 5660.
[2] T. Kobayashi, T. Okada, K.A. Nelson, S. De Silvestri, Ultrafast Phenomena XIV, Springer, New York, 2004.
[3] J.E. Sharping, M. Fiorentino, A. Coker, P. Kumar, Opt. Lett. 26 (2001) 1048.
[4] R.R. Alfano, Sci. Am. 295 (2006) 86.
[5] H. Walther, K.W. Rothe, Laser Spectroscopy IV, Springer, Berlin, 1979. p. 340.
[6] F. Théberge, N. Aközbek, W. Liu, A. Becker, S.L. Chin, Phys. Rev. Lett. 97 (2006) 023904.
[7] L. Misoguti, S. Backus, C.G. Durfee, R. Bartels, M.M. Murnane, H.C. Kapteyn, Phys. Rev. Lett. 87 (2001) 013601.
[8] T. Fuji, T. Horio, T. Suzuki, Opt. Lett. 32 (2007) 2481.
[9] T. Fuji, T. Suzuki, Opt. Lett. 32 (2007) 3330.
[10] A. Dubietis, G. Tamošauskas, P. Polesana, G. Valiulis, H. Valtna, D. Faccio, P. Di Trapani, A. Piskarskas, Opt. Express 15 (2007) 11126.
[11] H. Valtna, G. Tamošauskas, A. Dubietis, A. Piskarskas, Opt. Lett. 33 (2008) 971.
[12] H.K. Nienhuys, P.C.M. Planken, R.A. van Santen, Huib J. Bakker, Opt. Lett. 26 (2001) 1350.
[13] H. Crespo, J.T. Mendonça, A. Dos Santos, Opt. Lett. 25 (2000) 829.
[14] J. Liu, T. Kobayashi, Opt. Express 17 (2009) 4984.
[15] J. Liu, T. Kobayashi, Opt. Lett. 34 (2009) 1066.
[16] J. Liu, T. Kobayashi, Opt. Express 16 (2008) 22119.
[17] J. Liu, T. Kobayashi, Z. Wang, Opt. Express 17 (2009) 9226.
[18] M. Zhi, A.V. Sokolov, Opt. Lett. 32 (2007) 2251.
[19] E. Matsubara, T. Sekikawa, M. Yamashita, Appl. Phys. Lett. 92 (2008) 071104.
[20] H. Matsuki, K. Inoue, E. Hanamura, Phys. Rev. B 75 (2007) 024102.
[21] K. Inoue, J. Kato, E. Hanamura, H. Matsuki, E. Matsubara, Phys. Rev. B 76 (2007) 041101(R).
[22] E. Matsubara, K. Inoue, E. Hanamura, Phys. Rev. B 72 (2005) 134101.
[23] E. Matsubara, Y. Kawamoto, T. Sekikawa, M. Yamashita, Opt. Lett. (2009) 1837.
[24] J. Takahashi, E. Matsubara, T. Arima, E. Hanamura, Phys. Rev. B 68 (2003) 155102.
[25] J. Takahashi, M. Keisuke, Y. Toshirou, Opt. Lett. 31 (2006) 1501.
[26] M. Zhi, X. Wang, A.V. Sokolov, Opt. Express 16 (2008) 12139.
[27] J. Liu, J. Zhang, T. Kobayashi, Opt. Lett. 33 (2008) 1494.
[28] M. Zhi, A.V. Sokolov, New J. Phys. 10 (2008) 025032.
[29] J. Liu, T. Kobayashi, Opt. Lett. 34 (2009) 2402.
[30] A. Penzkofer, H.J. Lehmeier, Opt. Quant. Electron. 25 (1993) 815.
[31] J. Darginavičius, G. Tamošauskas, G. Valiulis, A. Dubietis, Opt. Commun. 282 (2009) 2995.
[32] R. Weigand, J.T. Mendonca, H. Crespo, Phys. Rev. A 79 (2009) 063838.
[33] Joao L. Silva, R. Weigand, H. Crespo, Opt. Lett. 34 (2009) 2489.
[34] A. Baltuška, M.S. Pshenichnikov, D.A. Wiersma, IEEE J. Quantum Electron. 35 (1999) 459.
[35] R. Trebino, Frequency-Resolved Optical Grating: The Measurement of Ultrashort Laser Pulses, Kluwer Academic Publishers, 2000. p. 279.

[36] B.D. Lü, Beam Characterization, Propagation and Transformation, Resonator Technology and Physics, third ed., Higher Education Press, Beijing, 2002. pp. 82–83, 105.
[37] Y. Fu, G. Feng, D. Zhang, J. Chen, S. Zhou, Optik (2009), doi:10.1016/j.ijleo.2008.08.003.
[38] P.B. Lundquist, D.R. Andersen, Y.S. Kivshar, Phys. Rev. E 57 (1998) 3551.
[39] G. Fanjoux, J. Michaud, M. Delqu'e, H. Mailotte, T. Sylvestre, Opt. Lett. 31 (2006) 3480.
[40] D. Polli, G. Cerullo, G. Lanzani, S. De Silvestri, K. Yanagi, H. Hashimoto, R.J. Cogdell, Phys. Rev. Lett. 93 (2004) 163002.
[41] D. Pestov, R.K. Murawski, G.O. Ariunbold, X. Wang, M.C. Zhi, A.V. Sokolov, V.A. Sautenkov, Y.V. Rostovtsev, A. Dogariu, Y. Huang, M.O. Scully, Science 316 (2007) 265.
[42] T. Brixner, J. Stenger, H.M. Vaswani, M. Cho, R.E. Blankenship, G.R. Fleming, Nature 434 (2005) 625.